On the determination of a cloud condensation nuclei from satellite: Challenges and possibilities

V. N. Kapustin,[1] A. D. Clarke,[1] Y. Shinozuka,[1] S. Howell,[1] V. Brekhovskikh,[1] T. Nakajima,[2] and A. Higurashi[3]

Received 18 October 2004; revised 6 October 2005; accepted 7 November 2005; published 21 February 2006.

[1] We use aerosol size distributions measured in the size range from 0.01 to 10+ μm during Transport and Chemical Evolution over the Pacific (TRACE-P) and Aerosol Characterization Experiment–Asia (ACE-Asia), results of chemical analysis, measured/modeled humidity growth, and stratification by air mass types to explore correlations between aerosol optical parameters and aerosol number concentration. Size distributions allow us to integrate aerosol number over any size range expected to be effective cloud condensation nuclei (CCN) and to provide definition of a proxy for CCN (CCN_{proxy}). Because of the internally mixed nature of most accumulation mode aerosol and the relationship between their measured volatility and solubility, this CCN_{proxy} can be linked to the optical properties of these size distributions at ambient conditions. This allows examination of the relationship between CCN_{proxy} and the aerosol spectral radiances detected by satellites. Relative increases in coarse aerosol (e.g., dust) generally add only a few particles to effective CCN but significantly increase the scattering detected by satellite and drive the Angstrom exponent (α) toward zero. This has prompted the use of a so-called aerosol index (AI) on the basis of the product of the aerosol optical depth and the nondimensional α, both of which can be inferred from satellite observations. This approach biases the AI to be closer to scattering values generated by particles in the accumulation mode that dominate particle number and is therefore dominated by sizes commonly effective as CCN. Our measurements demonstrate that AI does not generally relate well to a measured proxy for CCN unless the data are suitably stratified. Multiple layers, complex humidity profiles, dust with very low α mixed with pollution, and size distribution differences in pollution and biomass emissions appear to contribute most to method limitations. However, we demonstrate that these characteristic differences result in predictable influences on AI. These results suggest that inference of CCN from satellites will be challenging, but new satellite and model capabilities could possibly be integrated to improve this retrieval.

Citation: Kapustin, V. N., A. D. Clarke, Y. Shinozuka, S. Howell, V. Brekhovskikh, T. Nakajima, and A. Higurashi (2006), On the determination of a cloud condensation nuclei from satellite: Challenges and possibilities, *J. Geophys. Res.*, *111*, D04202, doi:10.1029/2004JD005527.

1. Introduction

[2] There is growing recognition of the importance of the ability of atmospheric aerosol to modify cloud properties (the aerosol indirect effects (AIE)) by acting as cloud condensation nuclei (CCN) and influencing the albedo, lifetime, precipitation and extent of clouds [*Albrecht*, 1989; *Heymsfield and McFarquhar*, 2001; *Hudson and Yum*, 2002; *Ramanathan et al.*, 2001; *Rosenfeld*, 2000; *Twomey*, 1991]. This has prompted substantial effort to detect and evaluate the AIE using models, in situ measurements, and satellite remote sensing [*Kaufman et al.*, 2002]. There have been a number of successful AIE observations using satellites. Such measurements include the aerosol retrieval products of the Advanced Very High Resolution Radiometer (AVHRR) [*Harshvardhan et al.*, 2002; *Nakajima et al.*, 2001; *Rudich et al.*, 2003; *Schwartz et al.*, 2002; *Sekiguchi et al.*, 2003], Sea-viewing Wide Field-of-view Sensor (SeaWiFS), Moderate Resolution Imaging Spectroradiometer (MODIS) [*Gassó and Hegg*, 2003; *Tanre et al.*, 1999], Polarization and Directionality of the Earth's Reflectances (POLDER) [*Bréon et al.*, 2002; *Deuze et al.*, 2000, 2001; *Mukai et al.*, 2003; *Quaas et al.*, 2004; *Rosenfeld*, 2000;

[1]Department of Oceanography, School of Ocean and Earth Science and Technology, University of Hawaii at Manoa, Honolulu, Hawaii, USA.
[2]Center for Climate System Research Center, University of Tokyo, Tokyo, Japan.
[3]Atmospheric Environment Division, National Institute for Environmental Studies, Ibaraki, Japan.

0148-0227/06/2004JD005527$09.00

Rosenfeld and Feingold, 2003; *Sekiguchi et al.*, 2003] and Tropical Rainfall Measuring Mission (TRMM) satellite [*Rosenfeld*, 2000].

[3] Satellite AIE observations can be divided into two groups. The first exploits the relationship between cloud droplet effective radius ($\mathbf{r_e}$) and cloud top temperature to explore how aerosols affect precipitation [*Rosenfeld*, 2000; *Rosenfeld et al.*, 2002; *Rudich et al.*, 2003]. The second group explores the $\mathbf{r_e}$–aerosol index (AI) relationship to study cloud droplet size and aerosol concentration [*Bréon et al.*, 2002; *Deuze et al.*, 2000, 2001; *Harshvardhan et al.*, 2002; *Kaufman et al.*, 2002; *Nakajima et al.*, 2001, 2003; *Quaas et al.*, 2004; *Sekiguchi et al.*, 2003; *Tanre et al.*, 1999]. Satellite observations show that $\mathbf{r_e}$ generally decreases in regions with high concentrations of pollution aerosol [*Bréon et al.*, 2002; *Nakajima et al.*, 2001; *Quaas et al.*, 2004; *Rosenfeld*, 2000; *Schwartz et al.*, 2002; *Sekiguchi et al.*, 2003], biomass burning [*Feingold et al.*, 2001], or dust [*Rosenfeld et al.*, 2001]. In contrast, the white Kuwait oil fires [*Rudich et al.*, 2003] or sea spray particles [*Rosenfeld et al.*, 2002] can be associated with an increase in $\mathbf{r_e}$.

[4] The aerosol index (AI) was defined [*Deuze et al.*, 2001] as the product of the satellite retrieved aerosol optical depth (AOD) and the Angstrom exponent α, AI = AOD $\cdot$ α. The spectral dependence of AOD is approximated by

$$\mathrm{AOD}(\lambda) = \mathrm{AOD}(\lambda_0)(\lambda/\lambda_0)^{-\alpha}, \quad (1)$$

where λ is wavelength. In the present study, satellite derived AOD(λ_0) is defined at a center wavelength λ_0 = 500 nm and an effective Angstrom exponent α is calculated using standard linear least squares fitting of AOD(λ) at five wavelengths in the range from 368 nm to 1050 nm (see section 2.2 below). Values of α are typically 1.5–2 for accumulation mode aerosol and approach zero for coarse dust, reflecting the wavelength dependence of the extinction coefficient in this wavelength region. As a result, AI is more sensitive than AOD to accumulation mode aerosol concentration, which is typically responsible for most CCN. In a later development it was suggested [*Nakajima et al.*, 2001] that satellite derived AI is positively correlated with column aerosol number concentration (column CN). Furthermore a negative correlation between $\mathbf{r_e}$ and column CN was shown. *Sekiguchi et al.* [2003] explored this approach to reveal the effects of column CN on $\mathbf{r_e}$, cloud optical and geometrical thickness, cloud fraction and cloud top temperature. At the same time recent analysis of the correlation between $\mathbf{r_e}$ and AI on the basis of climate model simulations [*Lohmann and Lesins*, 2002, 2003] reveal that this correlation is not unique and differs for continental and oceanic clouds.

[5] Observations of aerosol direct effects have been successfully pursued through a variety of satellite closure experiments [*Durkee et al.*, 2000; *Remer et al.*, 2002; *Ru et al.*, 2000; *Wang et al.*, 2003]. However, satellite studies of the AIE, especially the group exploiting the AI to column CN link, have little support from direct in situ measurements. This task is challenging because satellite observations are column effective measurements based on aerosol optical properties and are not directly dependent upon aerosol number concentration. The challenge with using satellite retrievals to study AIE is that in most cases CCN are too small to contribute much to observed radiances. Numerical model calculations have shown that the strong dependence of AOD and α on the aerosol size distribution parameters makes the column CN retrieval very difficult [*Feingold*, 2003; *Mishchenko et al.*, 2004]. Also there is an inherent error in the satellite aerosol retrieval methods that derives from the use of lognormal approximations with limited variability of size distribution parameters such as values of modal diameters, width and composition.

[6] Our aerosol size distributions measured over the size range from 0.01 to 10+ μm allow us to integrate aerosol number over any size range that is expected to be effective as CCN and provide a definition of $\mathrm{CCN_{proxy}}$. Using the results of chemical analysis [*Ma et al.*, 2004], measured/modeled humidity growth [*Howell et al.*, 2006] and stratification by air mass types we can calculate the optical properties of these size distributions at ambient conditions.

[7] The goal of this paper is to explore the relationship between AI and our defined $\mathrm{CCN_{proxy}}$ using aerosol data obtained during the Transport and Chemical Evolution over the Pacific (TRACE-P) and Aerosol Characterization Experiment–Asia (ACE-Asia) experiments. We then compare this in situ data to the approaches used for satellite (SeaWiFS) retrievals of column CN for the same region [*Higurashi and Nakajima*, 2002]. We emphasize that this paper is not intended to demonstrate "closure" between measured or inferred CCN and CCNproxy. It is rather an examination of measured aerosol properties that appear to have the greatest impact on the potential for satellites to derive CCN. In particular, we will demonstrate the effects of relative humidity (RH), mixed composition (dust, pollution, sea salt, biomass burning) and aerosol size distribution parameters on the relationship between AI and $\mathrm{CCN_{proxy}}$. Addressing these issues, though necessary, may not be sufficient for effective determination of CCN by satellite.

2. Data Sources

[8] In this paper we will use the data obtained during the TRACE-P and ACE-Asia experiments from three platforms: SeaWiFS satellite, the C-130 (ACE-Asia) and P-3B (TRACE-P) aircraft (Table 1). The following abbreviations and symbols are used in this and subsequent sections: AOD for satellite retrieved total column aerosol optical depth, σ_{ep} for extinction coefficient calculated from in situ or model size distributions, σ_{sp} for scattering coefficient measured by nephelometer, D_p for "dry" particle diameter, D_{act} for activation diameter, RH for relative humidity. The column aerosol number concentration (column CN, in $\mathrm{cm^{-2}}$) is calculated using the satellite retrieved aerosol size distribution parameters and is based upon assumed vertical column homogeneity. A proxy for in situ CCN concentration ($\mathrm{CCN_{proxy}}$, in $\mathrm{cm^{-3}}$) is defined as the integral of measured or modeled aerosol size distributions over a specified size range commonly activated in boundary layer clouds ($D_p > D_{act}$). Abbreviations N80nm and N100nm are used here for $\mathrm{CCN_{proxy}}$ with D_p > 80 nm and D_p > 100 nm. An effective Angstrom exponent α is calculated using retrieved or modeled bimodal size distribution parameters and Mie theory as a linear least squares fit of the aerosol extinction at wavelengths of 368, 500, 675, 862, and 1050 nm, chosen because they are widely used by Sun photometers (see

Table 1. Measured/Derived Quantities Included in This Study

Parameter	SeaWiFS	ACE/TRACE
Aerosol optical depth (AOD) or equivalent	AOD at λ = 500 nm, satellite retrieved	Extinction coefficient σ_{ep} (500) calculated using in situ or model size distributions; scattering coefficient σ_{sp} measured by nephelometer and adjusted to 500 nm
Aerosol size distribution	Retrieved bimodal lognormal distribution with C2/C1 ratio of peak values of coarse (C2) and accumulation (C1) volume modes; volume median diameters D1, D2, and geometric standard deviations σ1, σ2 (assumed)	Directly measured "dry" size distributions and in situ distributions calculated using RH growth with assumed composition
Angstrom exponent	Effective Angstrom exponent α, calculated using linear least squares fitting of the aerosol extinction at five regular Sun photometer wavelengths; aerosol extinction calculated using retrieved size distribution parameters	Effective Angstrom exponent α, calculated using linear least squares fitting of σ_{ep} (λ) at five regular Sun photometer wavelengths; α_{neph}, calculated using measured σ_{sp} at 450 and 700 nm
Aerosol index (AI)	Satellite-derived column AI: AI_{sat} = AOD $\cdot\alpha$	In situ or model size distribution-based AI: $AI_{dist} = \sigma_{ep} \cdot \alpha$; nephelometer AI: $AI_{meas} = \sigma_{sp} \cdot \alpha_{neph}$
Proxy for in situ CCN (CCN_{proxy})	Column number concentration (column CN), calculated using retrieved size distribution parameters and assuming vertical column homogeneity	Integral of measured size distribution over a size range commonly activated in boundary layer clouds ($D_p > D_{act}$); N80nm and N100nm are used for D_p > 80 nm and D_p > 100 nm

section 2.2). The nephelometer Angstrom exponent α_{neph} is calculated as

$$\alpha_{neph} = -\frac{\ln\left[\sigma_{sp}(\lambda_1)\Big/\sigma_{sp}(\lambda_2)\right]}{\ln\left[\lambda_1\Big/\lambda_2\right]}, \quad (2)$$

where λ_1 = 450 nm and λ_2 = 700 nm. Extinction or scattering coefficients are reported in Mm^{-1} (inverse megameters). The satellite derived column aerosol index (AI_{sat}) is defined as AI_{sat} = AOD $\cdot\alpha$. The in situ or model size distribution–based AI (AI_{dist}) is calculated as $AI_{dist} = \sigma_{ep} \cdot \alpha$; and the nephelometer based AI (AI_{scat}) is defined as $AI_{scat} = \sigma_{sp} \cdot \alpha_{neph}$, where AOD, σ_{ep} and σ_{sp} are taken at a center wavelength λ_0 = 500 nm.

2.1. TRACE-P and ACE-Asia Experiments

[9] The NSF ACE-Asia (ACE) and the NASA TRACE-P (TRACE) experiments took place over the western Pacific in March–April 2001 [*Huebert et al.*, 2003; *Jacob et al.*, 2003]. Nearly duplicate aerosol instrumentation compared favorably between the NASA P3-B (TRACE) and the NSF/NCAR C-130 (ACE) [*Moore et al.*, 2004]. This provided in situ data on aerosol optics and size distributions [*Clarke et al.*, 2004] that allow us to link optical properties to aerosol number. The combined size-resolved microphysics, optics and chemistry allow us to evaluate the derivation of column CN from SeaWiFS satellite observations [*Nakajima et al.*, 2001] (hereinafter referred to as N2001) using the *Higurashi and Nakajima* [1999] retrieval algorithm (hereinafter referred to as HN99). TRACE (intensive period 4 March to 4 April 2001) and ACE (31 March to 4 May 2001) provided an opportunity to investigate Asian outflow within the area 10°–45°N and 110°–155°E. Nearly 200 vertical profiles with altitude range of at least 3000 m were conducted (see Figure 1).

[10] A detailed description of the P3-B and C-130 aerosol instrumentation can be found in work by *Clarke et al.* [2004] and *Moore et al.* [2004]. Analysis of measured size distributions are discussed at length elsewhere [*Clarke et al.*, 2004] and the optical response to composition, humidity growth and refractive index are based on work by *Howell et al.* [2006]. In this paper we will be using aerosol size distributions and aerosol scattering properties.

2.1.1. Aerosol Size Distributions

[11] The fine aerosols (0.007 < D_p < 0.25 μm) were measured with a custom-made Radial Differential Mobility Analyzer (RDMA). Larger particles (0.1 < D_p < 10.0 μm) were sampled with a modified Laser Optical Particle Counter (OPC, PMS, Boulder, Colorado). Both the DMA and OPC were operated inside the aircraft near ambient pressure, but at cabin temperatures. The size distributions were measured after mixing with desiccated air to achieve "dry" conditions with sample RH in the range of 10–40% (we will be using notation RH = 30% in the text). The

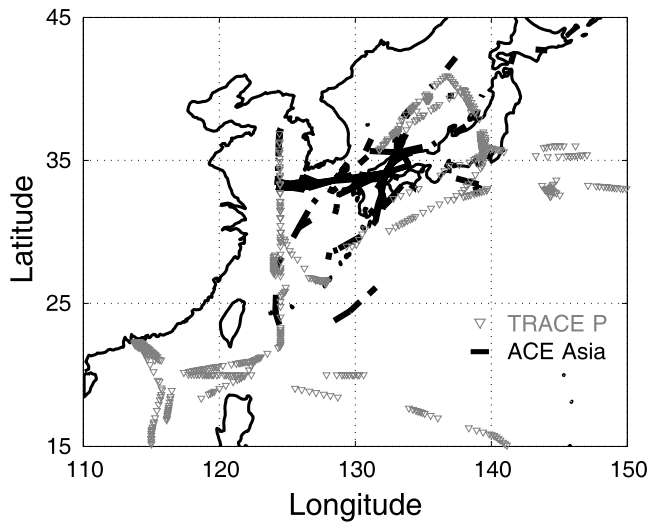

Figure 1. ACE and TRACE flight tracks for vertical profile segments with an altitude range >3000 m.

change in particle size as RH varies from 10 to 40% is small compared to our other size distribution measurement uncertainties. Drying reduces the impact of water uptake by the aerosol on the measured size so that the distributions reflect the aerosol components and not the water component [*Howell et al.*, 2006]. During horizontal legs the DMA and OPC operated with a thermal preconditioning unit that cycled the aerosol through 150°C and 350°C to drive off the volatile and semivolatile aerosol constituents, allowing inference of size-resolved aerosol chemistry [*Clarke*, 1991; *Howell et al.*, 2006].

2.1.2. Aerosol Scattering Properties

[12] The aerosol light scattering coefficients σ_{sp} were measured with TSI 3563 integrating nephelometers for λ = 450, 550, and 700 nm; corrected for truncation errors inherent in the instrument as per *Anderson et al.* [1996] and adjusted to the center wavelength λ_0 = 500 nm using α_{neph}. The nephelometer RH was typically below 45% and therefore the reported scattering coefficients are considered "dry." Aerosol optical properties are reported at ambient pressure and temperature.

2.2. Satellite Retrieval of Aerosol Optical and Microphysical Parameters

[13] A detailed description of the aerosol retrieval algorithm is given for AVHRR by HN99 and for SeaWiFS by *Higurashi and Nakajima* [2002]. Only a brief outline of the retrieval procedure is presented here. In the algorithm representative aerosol size distributions are assumed to be bimodal lognormal distributions,

$$\frac{dV}{d\log D_p} = \sum_{n=1}^{2} C_n \exp\left[-\frac{1}{2}\left(\frac{\log D_p - \log D_n}{\log \sigma_n}\right)^2\right], \qquad (3)$$

where V is the volume, D1, D2 and σ1, σ2 are the accumulation and coarse mode volume median diameters and geometric standard deviations respectively. *Higurashi and Nakajima* [1999] assumed D1 = 0.34 μm and D2 = 6.88 μm and geometric standard deviations σ1 = 1.96 and σ2 = 2.37 as the averages of size distributions reported by various authors between 1971–1991. Later [*Higurashi and Nakajima*, 2002; *Nakajima et al.*, 2001] the HN99 distribution was tuned with σ1 = 1.30 and σ2 = 2.75 to reduce a disagreement between theoretical and observed radiances. Two undetermined parameters in equation (3), peak values of the volume lognormal distributions C1 and C2, and the peak ratio C2/C1 can be determined from two-channel satellite radiances.

[14] Mie calculations for the coarse and accumulation modes are used to generate two lookup tables for nearly nonabsorbing and absorbing aerosols and to relate spectral radiances measured by SeaWiFS at 670 and 865 nm to the C2/C1 ratio and AOD at 500 nm. Hence the four-channel SeaWiFS aerosol retrieval algorithm is divided into two parts. First, the calculated radiances are compared with observed values at 670 and 865 nm and optimal values of AOD(500) and C2/C1 are searched. Second, a comparison between calculated and measured radiances at 412 and 443 nm is used to choose between the nonabsorbing and absorbing models. In this fashion, each set of four channel SeaWiFS radiances corresponds to a combination of AOD, C2/C1 and refractive index **m**.

[15] It should be noted that the peak ratio C2/C1, which represents the contribution of large particles, can be uniquely transformed to α. Although AOD, C2/C1 and **m** are the variables in the algorithm, the finally retrieved values are for AOD, wavelength mean α and **m**. In practice, wavelength-averaged α is obtained by a linear fit of the spectral aerosol extinction at regular Sun photometer wavelengths, 368, 500, 675, 862, and 1050 nm, calculated using assumed bimodal size distribution parameters. We will use the same definition for wavelength-averaged α in this paper except where otherwise mentioned. The column aerosol number concentration (column CN) is calculated using equation (3), under the assumption of a constant aerosol concentration from 0 to 3 km.

[16] This paper will examine the applicability of the following assumptions made by HN99 and N2001: (1) unique relation between α and C2/C1 ratio; (2) bimodality and lognormality of aerosol size distributions (accumulation and coarse modes); and (3) constancy of modal diameter, σ and **m** of each mode using our measured aerosol parameters.

[17] We note that increases in coarse aerosol (e.g., dust) generally do not add to CCN number [*Clarke et al.*, 2004] but significantly increase the scattering seen by satellite at longer wavelengths and drive the Angstrom exponent toward zero. This has prompted the use of the AI_{sat} to suppress the scattering contributed to AOD by coarse particles by multiplying AOD by α. Hence, although AOD can increase dramatically because of relatively few coarse aerosol, the AI_{sat} is less affected because of the factor α, thereby making AI_{sat} a better measure of aerosol number than AOD.

[18] Figure 2 shows the model N2001 (tuned) size distribution based SeaWiFS retrievals of AOD (gray area of Figure 2a) and AI_{sat} = AOD $\cdot\cdot\alpha$ (gray area of Figure 2b) versus column CN for the SeaWiFS swath collected on 25 April 2001 at 254 GMT for the area 15°–50°N and 130°–160°E. Colors highlight the AOD and AI_{sat} values obtained from satellite data for all locations and time periods from Figure 1 (ACE, blue and TRACE, red). This apparent linearity of AI_{sat} versus column CN forms the basis for using satellite radiances to estimate column CN. Examining the validity of this apparent linearity is the subject of this paper.

2.3. Calculations of in Situ Aerosol Size Distributions and Optical Parameters and CCN Proxy Definitions

[19] In order to simplify the calculation of in situ aerosol total scattering, extinction and Angstrom exponents from the size distributions we use a simplified version of ACE pollution (AAPO) mixture and algorithm described by *Howell et al.* [2006]. First the aerosol size distributions are divided into accumulation and coarse modes by finding the minima in volume distributions between 0.4 and 1 μm. The accumulation mode is then split into volatile and refractory fractions by using the accumulation mode volume lost after heating to 300°C or 350°C. The coarse mode is assigned a typical sea salt fraction during ACE (0.1 of coarse mode below 2 km and 0 above 2 km) and the remainder is assumed to be dust. The accumulation mode is assumed to be a typical internal mixture of the refractory and volatile components [*Clarke et al.*, 2004]. Hygroscopic

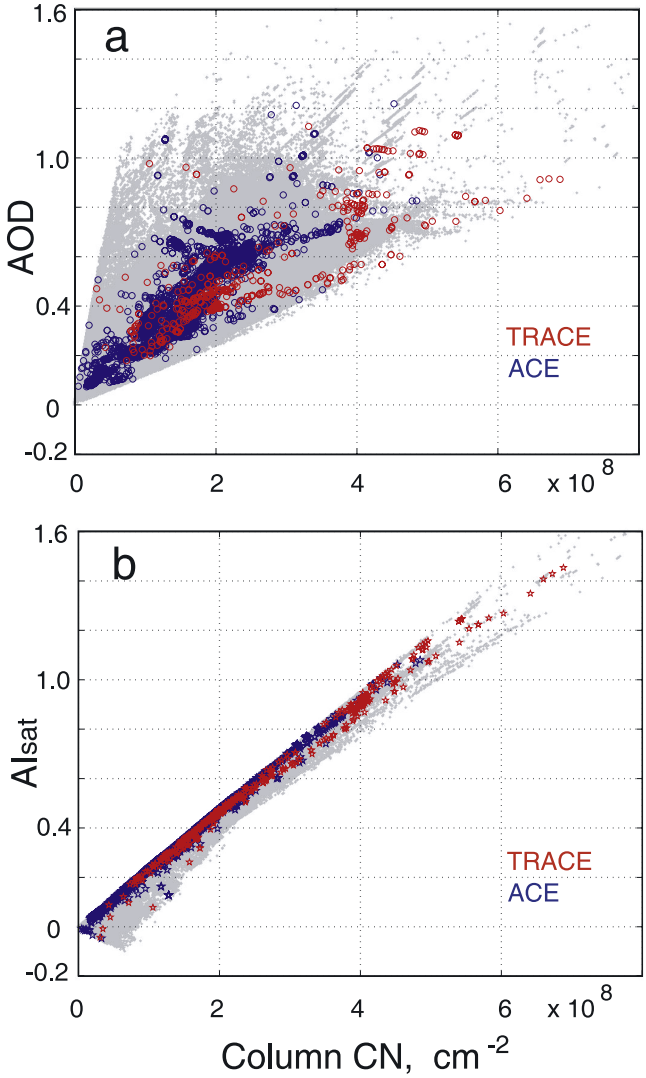

Figure 2. SeaWiFS retrieved (a) AOD and (b) AI_{sat} = AOD · α (gray) from swath collected on 25 April 2001 at 254 GMT for the area 15°–50°N and 130°–160°E versus retrieved column CN (all for the *Nakajima et al.* [2001] model). Colors highlight the AOD and AI_{sat} values obtained from satellite data for all locations and time periods from Figure 1 (ACE, blue; TRACE, red).

growth of each mode was calculated on the basis of the following assumptions: no RH growth for dust; sea salt growth follows *Tang et al.* [1997]; the volatile fraction of accumulation mode grows according to *Clarke et al.* [2002] with no growth for the refractory fraction of the accumulation mode. The accumulation mode refractive index was calculated as a mixture of the refractory fraction, primarily a mixture of soot and dust, and the volatile fraction, comprising organics, sulfates and water.

[20] We assume that the accumulation mode refractory fraction commonly has 50% soot and 50% dust-like aerosol (e.g., fly ash, dust tail, high-temperature organic carbon, etc) for calculation of optical properties. When dry, the volatile fraction is 25% organic carbon, and the remainder is assumed to be sulfate salts. Any additional volume at ambient RH is water. These simplifications allow us to infer the refractive index of each mode and, assuming particle sphericity, we can convert the measured OPC diameters to geometric diameter with equivalent Mie scattering and calculate the geometric diameters and optical parameters (scattering, extinction and α) at 30% RH and ambient RH. The last step allows us to calculate an aerosol index for our measured in situ data, AI_{dist}. Although this is a simplification of the aerosol chemistry and its variability during ACE, it captures the basic features.

[21] Next we will define a proxy for in situ CCN concentrations (CCN_{proxy}, in cm^{-3}) based upon integrating our measured dry size distributions over a size range commonly activated in boundary layer clouds. Precise calculations of the smallest dry particle diameter that activates in clouds (activation diameter D_{act}) require the use of complex relationships of applied supersaturation, particle size and chemistry and go well beyond the scope of this paper. We are not claiming our CCN_{proxy} is equivalent to in situ CCN of the same size. This would require "closure" studies that are not possible with the data available. Here we argue that our CCN_{proxy} has the approximate sizes and properties consistent with CCN that allow us to examine dependencies that impact the retrieval of CCN by satellite.

[22] To define a representative range of D_{act} we will use the values of the effective maximum cloud supersaturation (S) inferred from ground-based measurements of aerosol size distributions. This approach is based upon the frequently observed separation of the aerosol submicron size distribution into interstitial and cloud droplet residue modes (Hoppel minima) to estimate D_{act} and S [*Cantrell et al.*, 1999; *Hoppel et al.*, 1996; *Vong and Covert*, 1998]. The dry diameter at the minima reflects the lower-limit diameter for particles activated in cloud. These references indicate that this typically occurs in the range from 80 to 100 nm with inferred values of maximum supersaturation ranging from 0.1% to 0.3%. Some more direct measurements/inferences of the effective cloud supersaturation from direct CCN and cloud droplet measurements [*Hudson and Yum*, 2002; *Yum and Hudson*, 2005] typically showed similar range of the effective S values.

[23] The aerosol chemical composition is very important for defining particle cloud nucleating ability. We will use either 80 nm or 100 nm as D_{act} depending upon the instruments or data used. The 80 nm D_{act} implies that CCN_{proxy} is defined as aerosols that activate to become cloud droplets at 0.24% supersaturation for pure ammonium bisulfate [*Vong and Covert*, 1998], at ~0.25%–0.27% for complicated pollution mixture (MIXPO mixture, 70% of inorganic salts and 30% organic compounds) or at ~0.28%–0.32% for more complicated biomass burning composition mixture (MIXBIO, 30% of inorganic salts and 70% organic compounds) [*Rissler et al.*, 2004; *Svenningsson et al.*, 2005]. The 100 nm D_{act} value suggests 0.17% supersaturation for pure ammonium bisulfate, 0.18%–0.2% for MIXPO and ~0.2%–0.23% for MIXBIO mixture. Hence the CCN_{proxy} is dominated by particles in the accumulation mode. Because we have more OPC measurements with a lower limit of 100 nm we often use OPC-only size distributions to calculate CCN_{proxy} as an integral of dry (30% RH) size distributions in the size range

0.1 to 10 μm (N100nm). However, it is important to recognize that significant CCN may exist at smaller sizes. Hence we also discuss the less frequent combined DMA+OPC size distributions to characterize cases with an 80 nm D_{act}.

[24] One obvious approach to evaluate the AI method for column CN retrieval would be to integrate our in situ vertically resolved size distributions under suitable satellite images and then compare measured and retrieved column averaged CCN_{proxy} values. For a given regional aerosol type a constant ratio of AI to column CCN_{proxy} would imply satellite retrieval could be implemented. However, because the ACE and TRACE missions did not have this kind of closure experiment as an objective we have very few suitable opportunities for doing this. Even if a few coincident and complete cloud-free profiles were available near a satellite overpass, such comparisons would provide inadequate statistics. Instead we chose to explore the ratio AI_{dist}/CCN_{proxy} calculated for all measured (not column average) ACE and TRACE size distributions. For an idealized case of a vertically homogenous aerosol, this ratio would be the same as the ratio of column averaged measured AI_{dist} and CCN_{proxy}. Without the vertical homogeneity assumption the variations of our AI_m/CCN_{proxy} ratio represent the "range of possible observable values" of column average AI_{dist}/CCN_{proxy}. Ideally, a near constant ratio (slope of AI_{dist} versus CCN_{proxy}) would indicate a necessary (though perhaps not sufficient) condition for satellite retrieval of column CN. Clear trends or dependencies in the measured data that lead to variations in this ratio point to issues that must be resolved for satellite retrieval of CCN to be effective.

[25] For the analysis of our in situ size distribution data we use measured size distributions rather than lognormal fits as is often assumed for satellite retrieval. Hence we determine the in situ coarse (1 μm < D_p < 10 μm) mode to accumulation (D_p < 1 μm) mode volume ratio V2/V1 instead of the peak ratio, C2/C1, of the bimodal lognormal volume distribution estimated by HN99 and N2001. Figure 3 reveals that our volume ratio V2/V1 is linearly related to the peak ratio C2/C1 for the bimodal distributions of N2001 until coarse volumes (V2) exceed accumulation mode volumes (V1) by a factor of 20 or so (e.g., very high dust cases). The use of this formulation allows for the direct comparison of the retrieved SeaWiFS AI_{sat}/column CN data with the AI_{dist}/CCN_{proxy} calculated from measured size distributions (the use of AI_{dist}/CCN_{proxy} ratio eliminates altitude from column average values as it appears in the numerator and denominator). Hence studying the sensitivities of our AI_{dist}/CCN_{proxy} data provides a direct assessment of the corresponding sensitivities of the ratio AI_{sat}/column CN.

3. Aerosol Index and CCN Proxy

[26] Our full size distributions (particle diameters 10–10000 nm) require that the DMA and OPC provide coincident size distributions that can be combined. The DMA distributions are far fewer than the OPC distributions that have a lower limit of 100 nm. Hence we first consider a CCN_{proxy} defined at dry sizes larger than 100 nm (N100 nm, OPC data) in order to maximize the data points considered.

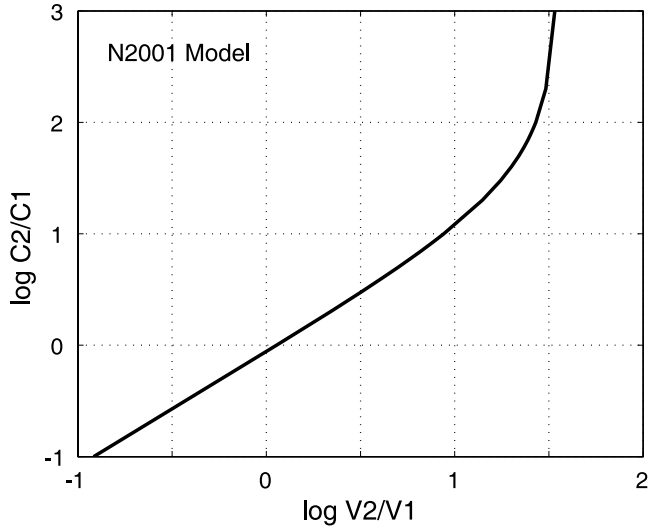

Figure 3. Comparison of volume ratio V2/V1 and peak ratio C2/C1 for bimodal size distributions based on N2001.

Later we will also discuss the combined distributions and their relation to a CCN_{proxy} with an 80 nm lower limit (N80nm). As an initial indication of the applicability of AI as a measure of CCN we plot AI_{meas} obtained only from the nephelometer. This is defined as the product of the dry nephelometer scattering at 500 nm and the Angstrom exponent determined at 450 and 700 nm, $AI_{meas} = \sigma_{sp} \cdot \alpha_{neph}$. This is plotted against the OPC measured CCN_{proxy} for sizes above 100 nm (N100nm) in Figure 4a for both ACE (blue) and TRACE (red) data. We note that these are for size distributions measured over 90 s only. The variability would be somewhat reduced by averaging over temporal scales of, say, 5 min (or about 25 km). However, for the analysis that follows we chose to maintain the high-resolution data in order to preserve variability in atmospheric aerosol fields. Even so, both data sets exhibit many cases that appear linear suggesting that AI_{meas} may be a useful indicator of CCN_{proxy}.

[27] Clearly the ACE data (Figure 4b) has far more scatter than the TRACE data (Figure 4c). Much of this will be shown to be due to the much higher dust concentrations common to ACE [*Clarke et al.*, 2004] and is similar to enhanced variability of AI_{sat} versus column CN relationship at large C2/C1 values on Figure 2 (ACE data points). We also note that the N100nm values above about 1500 cm^{-3} are in a range where the susceptibility of clouds to changes in CCN number is low. Hence the increased scatter evident at these higher concentrations has less influence on assessing any related impact on AIE. Consequently, the ability to resolve dependencies of CCN on AI at the lower range of concentrations is most important.

[28] Of course ambient atmospheric aerosol is not dry. Hence we have applied aerosol growth to these dry aerosol, as discussed above, on the basis of their being an internally mixed aerosol with a soluble component closely related to our measured aerosol volatility [*Howell et al.*, 2006]. These have been grown to sizes corresponding to ambient RH for each distribution and the resulting refractive index calculated. The same data shown in Figure 4a are plotted in Figure 4b

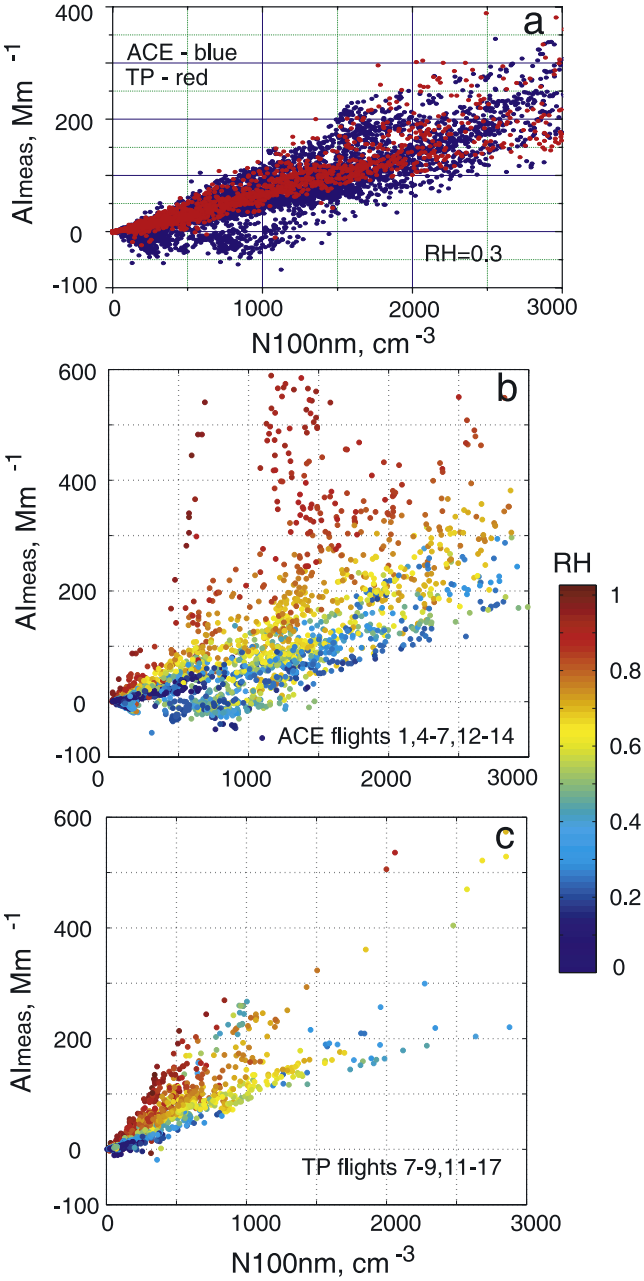

Figure 4. (a) ACE (blue dots) and TRACE (red dots) data for nephelometer AI_{meas} (σ_{sp}(500 nm) · $\alpha_{neph.}$ at 450 and 700 nm for nephelometer at 30% RH) versus N100nm (OPC at 30% RH). (b and c) Same as in Figure 4a but for AI_{meas} obtained only for OPC distributions at ambient RH for (b) ACE and (c) TRACE. Slope of AI_{meas} versus N100nm depends strongly on ambient RH.

for ACE and Figure 4c for TRACE where both are color coded with ambient RH for the same N100nm.

[29] Both data sets show that the relation between AI_{meas} and N100 nm is humidity dependent and that assumptions of a mean humidity will not provide a robust relation when integrated over the column unless RH is constant. However, the systematic increase of AI_{meas} with RH for a similar N100 nm values in both ACE and TRACE data suggests that an improved relation could be developed using an RH parameterization. The TRACE data also reveals that, under dry conditions, the tighter linear relation between ambient AI_{meas} and N100 nm appears promising. This is less evident in the ACE data largely because of the higher dust component during ACE and its strong effect on the Angstrom exponent in AI_{meas}. These influences on AI_{meas} indicate that similar impacts on satellite derived AI_{sat} can be expected.

4. Validity of Retrieval Assumptions

4.1. Calculated α Versus V2/V1

[30] As dust becomes a larger contributor to the aerosol size distribution it will drive the Angstrom exponent to lower values. This is evident for our in situ distributions when the calculated α is plotted against the volume ratio V2/V1 at ambient RH (Figure 5). Figure 5a shows this dependency along with the behavior expected for the non-absorbing (red line) and absorbing (black line) SeaWiFS retrieval models [*Higurashi and Nakajima*, 2002] and the average data from *Wang et al.* [2003] collected at Gosan, South Korea during ACE (black diamonds). The latter is consistent with our measured data and includes the negative α values that are present in ground-based in situ data for the ACE region [*Kim et al.*, 2004; *Markowicz et al.*, 2003]. The negative α values are not evident in the work by N2001 and are not common in satellite data or in direct column integration because column aerosol generally include enough altitudes that are influenced largely by accumulation mode aerosol to keep the column average α positive. In some cases, low α values for dust may also be removed because of aggressive cloud filtering algorithms [*Redemann et al.*, 2003].

[31] The low V2/V1 ratios reflect a dominant pollution aerosol with high Angstrom coefficient. The majority of lower α values were observed during heavy dust cases with typically low RH. The variability in the relationship at higher V2/V1 ratios is revealed by considering the data in Figure 5b. Here the data are color coded by altitude. The deviation from the N2001 relationship is obvious for high-altitude cases above 4 km. This can be explained by comparing the underlying optically effective size distributions to those employed by N2001. Figure 5c shows two dust events for ACE flight 13. All size distributions for high dust concentrations with V2 > 50 μm^3 cm^{-3} are normalized at 0.65 μm with a volume ratio V2/V1 > 10 and a low $\alpha < 0$ for altitudes <1 km (blue) and >4.5 km (red). The green line represents the M1 model size distribution for log (V2/V1) = 1.5. The M1 distribution captures the general shape of the in situ distributions. Overall, however, the measured ACE accumulation mode is wider than that of N2001. High-altitude dust for ACE flight 13 had a smaller coarse mode diameter D2 compared to low-altitude dust.

[32] In order to examine the effect of size distributions (with different D1, D2 and σ1, σ2) on α we calculated α for different bimodal distributions with parameters described in Table 2. The blue line in Figure 5b shows α versus V2/V1 for the M1 model using D1 and D2 similar to N2001 but with different σ1 and σ2. The yellow line shows a similar relationship for the M2 with a smaller D2. Both lines describe α versus V2/V1 dependency at large values of

V2/V1 (a prevailing coarse mode) reasonably well but with a faster decrease in α with increasing V2/V1 for model M2. Hence the deviations from N2001 are driven by smaller in situ values of D2 for high-altitude dust than that parameterized by N2001.

4.2. Bimodality and Lognormality of Aerosol Size Distributions

[33] It is important to recognize that the number distribution for CCN can include smaller sizes that tend to be high in number but have less influence on scattering [*Gassó and Hegg*, 2003]. Such CCN may contribute little to satellite derived radiance. Consequently, if satellite radiance is to be used to estimate CCN_{proxy} then these smaller sizes must scale with those sizes that contribute to ambient light scattering and satellite derived radiance. Measured aerosol size distributions in the majority of ACE and TRACE cases were bimodal and lognormal with the exception of strong pollution cases with enhanced smallest nuclei mode. Figure 6a shows combined OPC and DMA number distributions, dN/dlog D_p, when σ_{sp} at 550 nm > 20 Mm^{-1}. These include median and mean values for all ACE data (blue lines) and those cases with elevated concentrations of ultrafine condensation nuclei (3 to 10 nm) greater than 4000 particles cm^{-3} (red lines). High concentrations of nuclei and Aitken mode aerosols were typically measured downwind of urban industrial sources in Asia after 12–48 hours of transport. These secondary aerosols only contributed a small percentage of new numbers to the accumulation mode aerosol above 80 nm for all cases including elevated nuclei mode cases. The latter were estimated to be significant in only about 15% of total measurements during ACE [*McNaughton et al.*, 2004].

[34] The particles larger than 80 nm or 100 nm are both part of the accumulation mode. This relationship is also consistent with the evidence that the accumulation mode number is established by emission of combustion derived black carbon aerosol upon which other volatile and soluble species condense [*Clarke et al.*, 2004]. This proportionality is evident in Figure 6b where the number concentrations larger than 100 nm (N100nm) are plotted against those larger than 80 nm (N80nm). These concentrations differ by less than 15%. Unusually higher N80nm concentrations (larger than 4000) are associated with unusually high pollution episodes. This confirms that generally the CCN in the 80–100 nm sizes (not sensed directly by satellites) track with the larger sizes that dominate the radiances.

4.3. Constancy of Modal D1, D2, σ1, σ2, and m

[35] The HN99 and N2001 models and other satellite retrievals assume that aerosol size distributions, composition and ambient RH (or RH growth of particles) are constant throughout the column, which is not a good assumption for the regional-scale retrievals needed for AIE assessments. We already mentioned that the accumulation mode mean diameter and index of refraction are strong functions of RH. Coarse mode diameter [*Kim et al.*, 2004] and standard deviations of coarse (Figure 5c) and

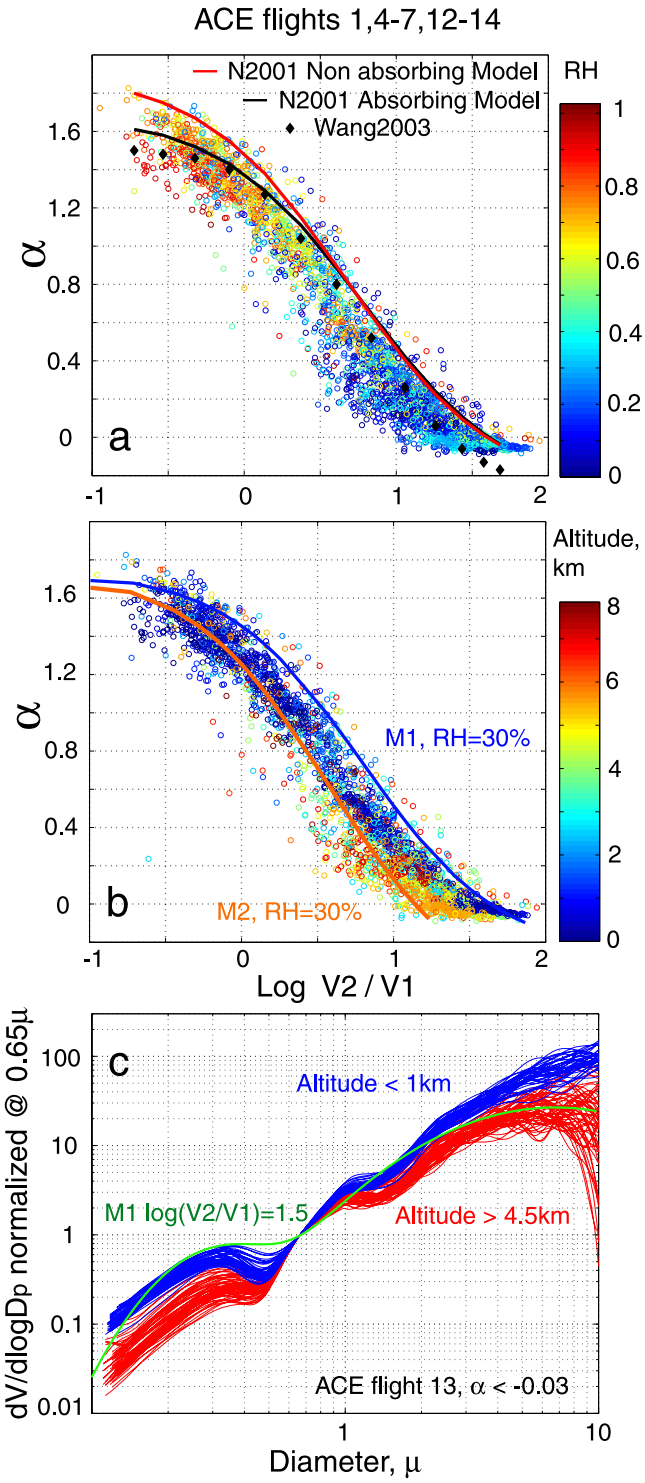

Figure 5. (a) Comparison of α versus V2/V1 for ACE OPC ambient RH size distributions (dots) and SeaWiFS retrievals (lines) color coded by RH: black diamonds, ACE data from Gosan 18-day average size distributions [*Wang et al.*, 2003]; lines, global mean from *Nakajima et al.* [2001] (red, nonabsorbing and black, absorbing models). (b) Same as in Figure 5a but color coded by altitude: lines, α versus V2/V1 calculated for M1 (blue) and M2 (yellow) models (see section 5). (c) ACE flight 13 size distributions dV/dlog D_p normalized at 0.65 μm below 1 km (blue lines) and above 4.5 km (red lines); green line, model M1 distribution for log (V2/V1) = 1.5.

Table 2. Bimodal Lognormal Distribution Parameters[a]

Model	D1, μm	D2, μm	σ1	σ2	Composition	D_{act}, μm	RH
HN99	0.34	6.88	1.96	2.37	HN99	0.1	No RH growth
N2001	0.34	6.88	1.30	2.75	N2001	0.1	No RH growth
M1	0.34	6.88	1.60	2.37	AAPO	0.1	0.3, 0.9
M2	0.34	4.88	1.60	2.37	AAPO	0.1	0.3, 0.9
M3	0.50	6.88	1.60	2.37	AAPO	0.1	0.3, 0.9
M3	0.50	6.88	1.60	2.37	MIXBIO	0.1	0.9

[a]D1 and D2 are volume median diameters of modes 1 and 2, respectively; σ1 and σ2 are geometric standard deviations of modes 1 and 2, respectively; D_{act} is activation diameter; RH is relative humidity; AAPO is the ACE-Asia pollution composition model [*Howell et al.*, 2006]; and MIXBIO is biomass burning composition [*Svenningsson et al.*, 2005].

accumulation modes [*Rissler et al.*, 2004; *Zhou et al.*, 2002] can also vary on regional scales.

5. Discussion

[36] The ratios AI_{dist}/CCN_{proxy} and AI_{sat}/column CN both attempt to relate aerosol optics to CCN number. The first reflects the in situ ambient size distribution while the latter reflects the column effective size distribution. Near constant ratios imply conditions when CCN_{proxy} can be derived from satellite observations. Therefore by examining the factors that influence the in situ ratio we can identify the factors that influence the satellite ratio. Figure 7 shows the in situ AI_{dist}/N100nm ratio plotted against log (V2/V1) for the more frequent OPC data. The log format is used to capture the full dynamic range of the data. Figure 7 demonstrates that the major uncertainties in using the N2001 approach to obtain CCN_{proxy} are linked to the issues of aerosol growth in response to varying humidity (red points) and to larger dust events that lead to very low Angstrom exponents (V2/V1 $\gg$ 1). This suggests that the HN99 and N2001 assumption of fixed mode diameters scaled only by C1 and C2 cannot adequately capture the in situ aerosol variability (a function of RH) and their associated optical properties.

[37] In order to examine the sensitivity of the relation of AI and CCN_{proxy} to size distribution parameters, particle composition and related particle properties (e.g., size growth with RH and aerosol activation diameter) we calculate AI_{dist}/CCN_{proxy} as a function of V2/V1 using the different bimodal distribution models shown in Table 1. The HN99 and N2001 models were described earlier (see section 2.2) with a constant D and σ and without any RH growth. For these models we use D_{act} = 100 nm. To describe ACE pollution aerosol we use the M1 model. The M1 model parameters are similar to HN99 but with a smaller σ1 of the accumulation mode. The composition and RH growth of this mode (ACE pollution composition (AAPO)) is described by *Howell et al.* [2006]. For this model we also use D_{act} = 100 nm. The M2 model parameters are similar to M1 but with smaller D2 of the coarse mode. This model describes ACE high-altitude dust mode diameter changes in Figure 5c. The composition, RH growth and D_{act} of this model are the same as for M1. The TRACE biomass burning aerosol is described by the M3 model. The M3 model parameters are similar to M1 but with a larger D1 for the accumulation mode. The choice of composition and RH growth of this mode MIXBIO is based upon measurements for biomass emissions described by *Svenningsson et al.* [2005]. For this model we also use D_{act} = 100 nm.

[38] Results from the calculations of AI_{dist}/N100nm versus V2/V1 ratio are shown in Figure 8. The black line corresponds to the HN99 model. The green line corresponds to the N2001 model. All blue lines are for model results at "dry" conditions with RH = 0.3. Red and yellow lines correspond to results at RH = 0.9 and represent the

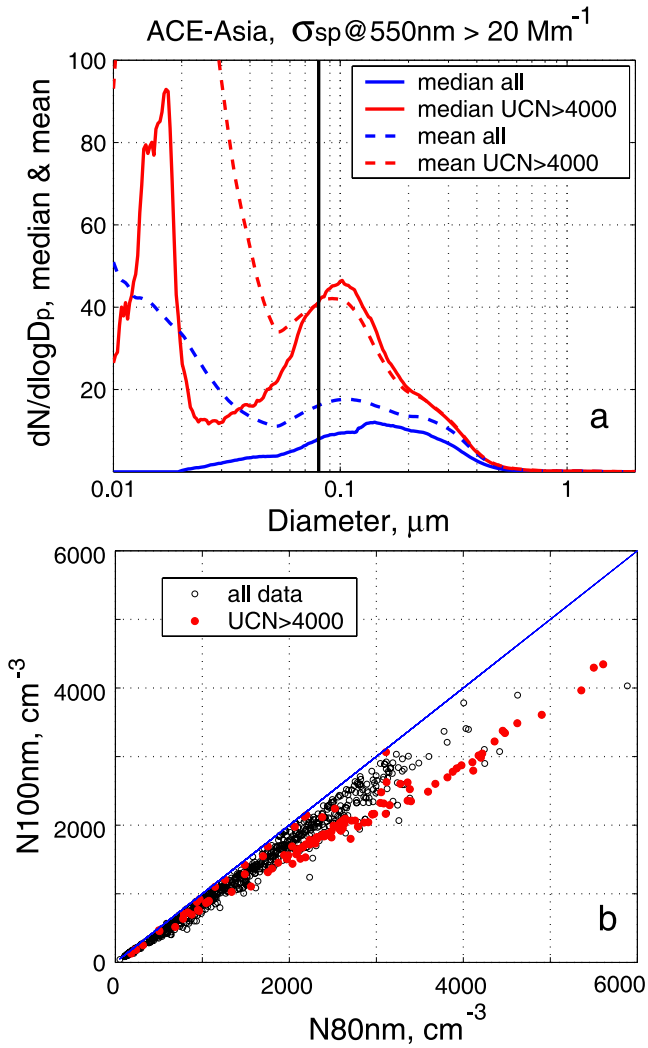

Figure 6. (a) ACE mean and median number size distributions for all distributions (blue) and for group with ultrafine condensation nuclei (UCN) greater than 4000 (red). (b) Comparison of N80nm with N100nm; red dots represent group with UCN > 4000.

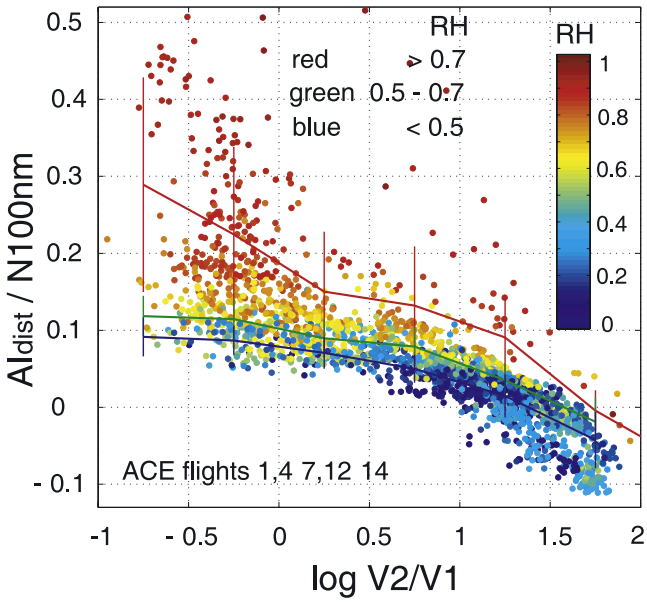

Figure 7. AI_{dist}/N100nm versus log V2/V1 for all ACE size distributions color coded by ambient RH. Colored lines represent AI_{dist}/N100nm averaged over RH bins of RH < 0.5, 0.5 < RH < 0.7, and RH > 0.7. Vertical lines represent standard deviation of data within each log (V2/V1) = 0.5 volume ratio interval.

maximum range in RH expected in noncloudy air. The frequency of ambient RH values observed during ACE are evident in the cases shown in Figure 7 but column average values will vary significantly less. Arrows (see Figure 8) show increases in AI_{dist}/N100nm ratio with RH (RH growth, blue) and in response to differences in modal diameters of size distributions (D1 and D2 increase, black) as well as differences in particle composition (composition, black).

[39] The largest changes in the AI_{dist}/N100nm ratio are due to the large RH growth indicated for the accumulation mode particle diameters (blue arrows). The AI_{dist}/N100nm ratio for AAPO changes from near 0.09 at RH = 0.3 (blue dashed and dotted lines for the M1 and M2 models) to ~0.24 (red solid and dotted lines for M1 and M2) at RH = 0.9. For AAPO composition and the M3 model the ratio changes from 0.19 at RH = 0.3 (blue dash-dotted line) to ~0.43 (red dash-dotted line) at RH = 0.9. For MIXBIO composition and M3 model the ratio changes from 0.19 at RH = 0.3 (blue dash-dotted line) to ~0.38 (yellow solid line). Changes in AI_{dist}/N100nm due to increase of D1 or/and D2 are also large (black arrows). The relative impact of composition on D_{act} (magenta lines and symbols) on the AI_{dist}/N100nm ratio is smaller than the illustrated changes in RH growth or aerosol modal diameter.

[40] The variations in RH, size distribution parameters, composition and D_{act} are related to variation in AI_{dist}/CCN_{proxy} (AI_{dist} to CCN_{proxy} slope) and provide some measure of the error associated with the retrieval of CCN_{proxy} from AI. Clearly these changes could result in very different values for the ratio of AI_{sat} to the column CN and help explain the variability in Figure 7. However, these properties will be expressed differently over the column seen by the satellite. This is particularly true for RH that may vary over the range of 0.3 to 0.9 somewhere in the column. However, often most of the extinction will be associated with smaller variations around a mean RH with only relatively narrow regions in the vertical that may have values near 0.9 (e.g., near the inversion). Consequently, the wide range in AI_{dist}/N100nm measured for in situ cases in Figure 7 will generally be much reduced in the column weighted AI_{sat}/column CN obtained by satellite. Similar reductions may also apply to size and compositional effects for satellite data due to multiple layers with different characteristics but unless these variations can be distinguished in some way resulting uncertainties in retrieved CCN could be considerable.

[41] Figure 8 also demonstrates that model aerosol size distribution parameters in the HN99 model capture only "dry" aerosol AI_{dist}/N100nm versus V2/V1 variability (black solid curve), whereas the N2001 model (green curve) better reflects variability under high humidity. Figure 9a also illustrates this variability in terms of aerosol types measured during ACE. We have identified the data shown in Figure 7 associated with cases of high humidity (RH > 75%, red), moderate to high light absorption as a pollution indicator (>1 Mm^{-1}, blue), and high dust in the absence of pollution (black) against a background of all other measured values (open circles). The blue line represents the model M1 (coarse mode diameter D2 = 6.88 μm), and the black line represents the model M2 (D2 = 4.88 μm). This becomes more clear if we plot the linear ratio of V2/V1 (Figure 9b) where 0 < V2/V1 < 20 (i.e., coarse aerosol does not exceed 20 times the volume of the accumulation mode aerosol). In spite of the natural variability associated with these 90 s measurements, a fairly robust dependency of the ratio is evident for the pollution and dust mix when RH is below

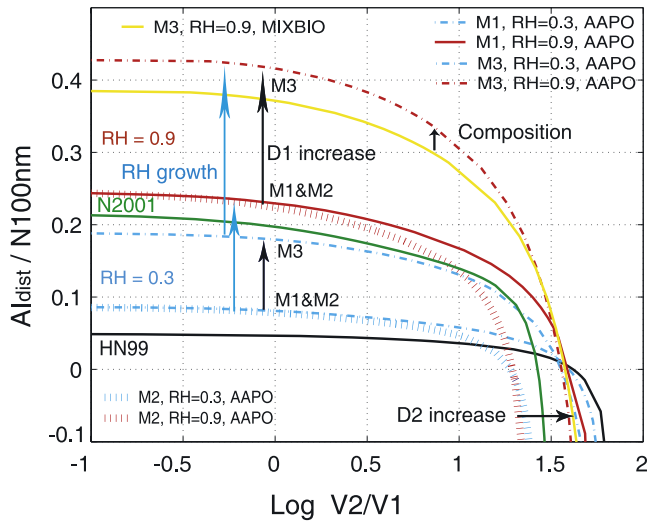

Figure 8. AI_{dist}/N100nm versus V2/V1 ratio calculated for bimodal lognormal distributions (see Table 1). Black line is from *Higurashi and Nakajima* [1999]. All blue lines are for RH = 0.3. Green line is from *Nakajima et al.* [2001]. Red and yellow lines correspond to RH = 0.9. Arrows show AI_{dist}/N100nm variability with RH (RH growth is shown in blue), modal diameters of size distribution (D1 and D2 increases are shown in black), and particle composition (also shown in black).

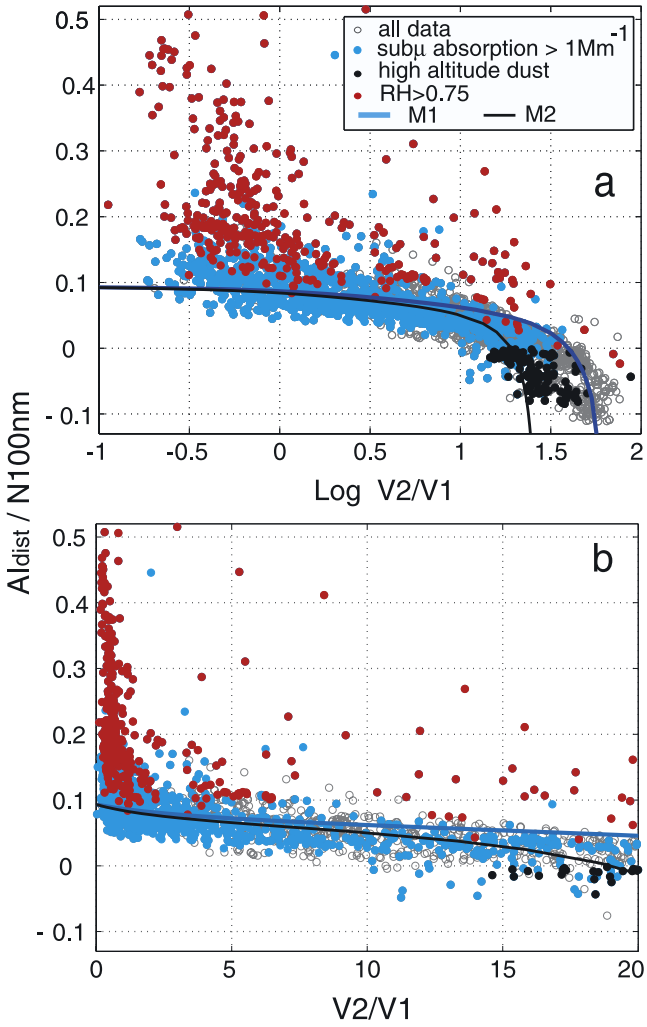

Figure 9. Measured AI_{dist}/N100nm for different aerosol types: cases of high humidity (RH > 75%, red), moderate to high light absorption as a pollution indicator (>1 Mm^{-1}, blue), and high dust in the absence of pollution (black) against a background of all other measured values (open circles). Blue line represents model M1 (coarse mode diameter D2 = 6.88 μm), and black line represents model M2 (D2 = 4.88 μm).

75% (compare to model M1 and M2, blue and black curves). These observations indicate that if suitable techniques are used to stratify satellite data into similar types and/or conditions then progress could be made in linking satellite radiances to CCN.

[42] The above plots have focused upon ACE data because it included pollution, dust and variable RH environments. However, the TRACE data set has more data south of 25N that included significant biomass combustion sources [*Carmichael et al.*, 2003; *Ma et al.*, 2003; *Tang et al.*, 2003; *Zhang et al.*, 2003]. Hence it is valuable to compare these cases to the ACE data for any similarities and differences. This is done in Figures 10a and 10b where we plot the AI_{dist} to N100nm ratio as a function of RH for both data sets. In Figure 10a the ACE data are color coded by α and fits are shown for data present in each of the 4 ranges indicated for α. Here more pollution with high α is colored more red and dust more blue. These ratios are nearly horizontal for RH below about 60% and suggest an improved ability to retrieve CCN_{proxy} from the satellite data if it were stratified additionally into values of α.

[43] A histogram of the values for RH corresponding to the data shown is included as gray bars in the background of

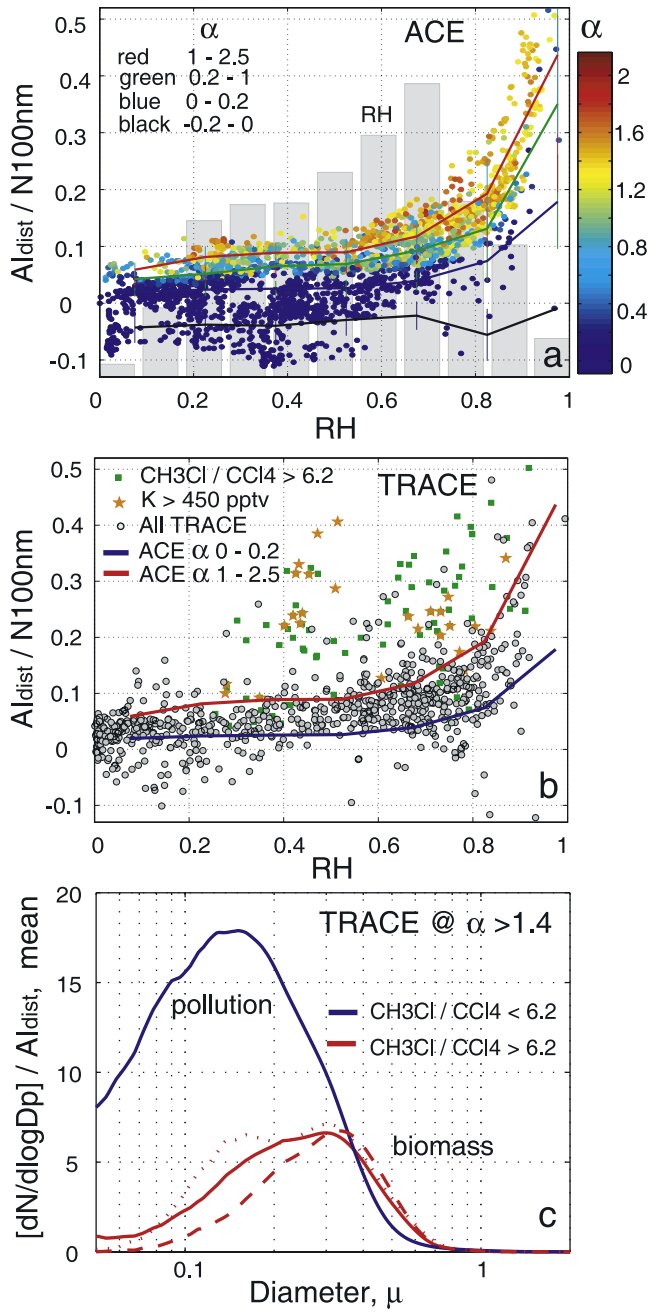

Figure 10. AI_{dist}/N100nm ratio as a function of RH (a) color coded by α for ACE and (b) color coded by biomass burning indicators for TRACE. (c) TRACE mean size distributions normalized by AI for biomass (solid red line) and typical pollution plumes (blue line). Biomass burning size distributions often combine both biomass (dashed red line) and pollution modes (dotted red line). A histogram of the values for RH corresponding to the data shown is included as gray bars in the background of Figure 10a.

Figure 10a. The most frequent RH near 70% is commonly expected over this altitude range [*Peixoto and Oort*, 1996]. Marked deviations from a horizontal line grow as RH increases above about 60% and these data points represent about one third of our ACE data for the altitudes below 2 km, the altitude range that generally dominates column optical depth during ACE [*Clarke et al.*, 2004; *Redemann et al.*, 2003]. The dramatic increase in the slope of AI_{dist}/N100nm reflects the strong nonlinearity in the hygroscopic growth factor for total particle scattering f(RH). At 90% RH the same number of particles can generate 3 times the scattering than at 50% RH. While such high RH values seldom reflect column average humidity below 2 km they frequently exist over more limited altitude regions and can have a disproportionate contribution to column radiances detected by satellite. However, if independent data on RH (e.g., meteorological models, radiosondes, AIRS satellite etc.) and on vertical aerosol structure (e.g., spaceborne lidar) were available then even cases of higher RH could be parameterized in terms of the satellite derived AI and Angstrom exponent. Eliminating consideration of cases with very low α (very high dust) would also improve the relationship.

[44] The TRACE data is shown in Figure 10b and here the color coding has been changed to reveal cases of biomass burning influence on the basis of *Ma et al.* [2003]. Here we use CH_3Cl/CCl_4 ratio and potassium (K) values as biomass burning indicators. The red and blue lines express the same ranges of α shown in Figure 10a and are included for reference. Because less dust (low α) was observed during TRACE, these lines embrace most of the data. Interestingly, for a broad range of RH values the biomass burning cases (color highlighted) have a significantly higher AI_{dist} to N100nm ratio than the more typical mixed pollution data (black circles). This difference means that a given measured AI_{dist} corresponds to fewer N100nm in biomass plumes than it does in typical pollution plumes.

[45] The reason for this is evident in the size distributions shown in Figure 10c for biomass burning plumes (solid red line) with $CH_3Cl/CCl_4 > 6.2$, $\alpha > 1.4$ and σ_{sp} at 550 nm > 20 Mm^{-1} and the more typical pollution plumes (blue line) with $CH_3Cl/CCl_4 < 6.2$. These data are plotted as the average number distributions per unit associated AI_{dist}. In other words, the larger the area under the curve then the greater number of particles for a given AI_{dist} value. This confirms that the biomass plumes have far fewer particles for the observed AI than the mixed pollution aerosol. Hence satellite retrievals of CCN_{proxy} from AI will have to be stratified for relationships consistent with the plume type expected to be present. The biomass burning aerosol size distributions peak at larger diameters and are generally narrower distributions than those measured in polluted air masses [*Eck et al.*, 2003; *Ogunjobi et al.*, 2004; *Zhou et al.*, 2002]. This appears to be linked to the nature of the combustion process and differences in the production of the primary sizes of black carbon in both sources [*Clarke et al.*, 2004].

6. Conclusions

[46] We have examined aerosol data from two extensive aircraft campaigns in 2001 (ACE and TRACE) over the western Pacific in order to explore the potential for using satellite radiances to describe an aerosol index (AI) able to remotely characterize the aerosol column number concentration and related CCN. We have done this by looking at the relationship between the measured in situ AI and the associated particle number larger than sizes typically effective as CCN (e.g., 100 nm). Here we used AI defined as the product of ambient light extinction at λ = 500 nm and the Angstrom exponent, although other formulations are possible. We identified the key issues and limitations of approaches similar to those suggested by N2001 but also provide guidance on how data stratification, integration of ancillary data and the separate application to certain aerosol types might improve satellite retrieval of CCN_{proxy}.

[47] The N2001 approach employs a bimodal size distribution at two fixed diameters that are fit to observed spectral radiance by allowing the volume mode amplitudes to vary. We demonstrate that this can capture many features of the aerosol optics but can often lead to incorrect estimates of the associated column particle number. It appears best suited to pollution aerosol with moderate amounts of coarse dust. However, the fixed mode diameters do not allow it to properly capture the pollution mode aerosol under higher relative RH (above about 75%) or aerosol dominated by high dust concentrations. The two geometric standard deviations used by HN99 (1.96) and N2001 (1.3) (see Table 2) provide an indication of the sensitivity of the model to this parameter. The measurement-based value of 1.6 used here provides a better fit to the data (Figure 8). There also appears to be a systematic difference in aerosol size distributions for Asian pollution and biomass burning plumes that lead to different relationships between AI and CCN_{proxy} (Figure 9). This suggests some a priori information on aerosol type may need to be included in the retrieval (e.g., CTM model input or region-specific retrievals).

[48] The limitations in retrieving CCN revealed by this analysis for the SeaWiFS satellite clearly represent a challenge. However, our analysis does suggest that suitable stratification of the aerosol types based on ancillary information could improve satellite retrievals of CCN_{proxy}. This information should include the relation between aerosol layers and RH [*Carrico et al.*, 2003; *Howell et al.*, 2006], greater spectral flexibility in assessing the Angstrom coefficient and utilization of variable mode diameters and standard deviations for the size distributions used in the retrieval algorithm. Improved satellite and model capabilities that are now becoming available could provide integrated data to facilitate this type of assessment [*Mishchenko et al.*, 2004].

[49] New generation satellites can now provide concurrent spectral radiances that can be inverted to get more realistic size distributions [*Chu et al.*, 2003]. These can be linked to vertically resolved aerosol layers using spaceborne lidar, remote sensing of relative humidity profiles, and detection of trace gases characteristic of different emission sources. These capabilities can be coupled to rapidly evolving chemical transport models that can include the growing quantitative understanding of in situ aerosol growth in response to embedded RH fields. Integration of these products would provide much improved constraints on retrievals that should lead to better characterization of ambient CCN and their link to remotely sensed cloud properties. Confirmation of this capability would need to go beyond the scope of this

investigation and include carefully focused closure studies needed to establish the link between ambient CCN and the CCN_{proxy} employed here. However, we believe that this assessment characterizes the nature and magnitude of the issues to be overcome and supports continued pursuit of this objective in order to employ satellites to evaluate CCN and related AIE objectives.

[50] **Acknowledgments.** The data analysis for this paper was carried out with NASA support under award NNG04GB39G. The data used here were obtained through grants provided for our participation in the TRACE-P (NASA NCC-1-416) and ACE-Asia (NSF ATM00-02070) experiments. The authors would like to thank all the members of the ACE-Asia and TRACE-P team and Barry Huebert, Daniel Jacob, and James Crawford for their leadership during these campaigns. This is SOEST contribution 6692.

References

Albrecht, B. A. (1989), Aerosols, cloud microphysics, and fractional cloudiness, *Science*, *245*(4923), 1227–1230.

Anderson, T. L., et al. (1996), Performance characteristics of a high-sensitivity, three-wavelength, total scatter/backscatter nephelometer, *J. Atmos. Oceanic Technol.*, *13*(5), 967–986.

Bréon, F. M., D. Tanre, and S. Generoso (2002), Aerosol effect on cloud droplet size monitored from satellite, *Science*, *295*(5556), 834–838.

Cantrell, W., G. Shaw, and R. Benner (1999), Cloud properties inferred from bimodal aerosol number distributions, *J. Geophys. Res.*, *104*(D22), 27,615–27,624.

Carmichael, G. R., et al. (2003), Regional-scale chemical transport modeling in support of the analysis of observations obtained during the TRACE-P experiment, *J. Geophys. Res.*, *108*(D21), 8823, doi:10.1029/2002JD003117.

Carrico, C. M., P. Kus, M. J. Rood, P. K. Quinn, and T. S. Bates (2003), Mixtures of pollution, dust, sea salt, and volcanic aerosol during ACE-Asia: Radiative properties as a function of relative humidity, *J. Geophys. Res.*, *108*(D23), 8650, doi:10.1029/2003JD003405.

Chu, D. A., Y. J. Kaufman, G. Zibordi, J. D. Chern, J. Mao, C. Li, and B. N. Holben (2003), Global monitoring of air pollution over land from the Earth Observing System-Terra Moderate Resolution Imaging Spectroradiometer (MODIS), *J. Geophys. Res.*, *108*(D21), 4661, doi:10.1029/2002JD003179.

Clarke, A. D. (1991), A thermo optic technique for in-situ analysis of size-resolved aerosol physicochemistry, *Atmos. Environ., Part A*, *25*(3–4), 635–644.

Clarke, A. D., et al. (2002), INDOEX aerosol: A comparison and summary of chemical, microphysical, and optical properties observed from land, ship, and aircraft, *J. Geophys. Res.*, *107*(D19), 8033, doi:10.1029/2001JD000572.

Clarke, A. D., et al. (2004), Size distributions and mixtures of dust and black carbon aerosol in Asian outflow: Physiochemistry and optical properties, *J. Geophys. Res.*, *109*, D15S09, doi:10.1029/2003JD004378.

Deuze, J. L., P. Goloub, M. Herman, A. Marchand, G. Perry, S. Susana, and D. Tanre (2000), Estimate of the aerosol properties over the ocean with POLDER, *J. Geophys. Res.*, *105*(D12), 15,329–15,346.

Deuze, J. L., et al. (2001), Remote sensing of aerosols over land surfaces from POLDER-ADEOS-1 polarized measurements, *J. Geophys. Res.*, *106*(D5), 4913–4926.

Durkee, P. A., et al. (2000), Regional aerosol optical depth characteristics from satellite observations: ACE-1, TARFOX and ACE-2 results, *Tellus, Ser. B*, *52*(2), 484–497.

Eck, T. F., et al. (2003), Variability of biomass burning aerosol optical characteristics in southern Africa during the SAFARI 2000 dry season campaign and a comparison of single scattering albedo estimates from radiometric measurements, *J. Geophys. Res.*, *108*(D13), 8477, doi:10.1029/2002JD002321.

Feingold, G. (2003), Modeling of the first indirect effect: Analysis of measurement requirements, *Geophys. Res. Lett.*, *30*(19), 1997, doi:10.1029/2003GL017967.

Feingold, G., L. A. Remer, J. Ramaprasad, and Y. J. Kaufman (2001), Analysis of smoke impact on clouds in Brazilian biomass burning regions: An extension of Twomey's approach, *J. Geophys. Res.*, *106*(D19), 22,907–22,922.

Gassó, S., and D. A. Hegg (2003), On the retrieval of columnar aerosol mass and CCN concentration by MODIS, *J. Geophys. Res.*, *108*(D1), 4010, doi:10.1029/2002JD002382.

Harshvardhan, S. E. Schwartz, C. M. Benkovitz, and G. Guo (2002), Aerosol influence on cloud microphysics examined by satellite measurements and chemical transport modeling, *J. Atmos. Sci.*, *59*(3), 714–725.

Heymsfield, A. J., and G. M. McFarquhar (2001), Microphysics of INDOEX clean and polluted trade cumulus clouds, *J. Geophys. Res.*, *106*(D22), 28,653–28,674.

Higurashi, A., and T. Nakajima (1999), Development of a two-channel aerosol retrieval algorithm on a global scale using NOAA AVHRR, *J. Atmos. Sci.*, *56*(7), 924–941.

Higurashi, A., and T. Nakajima (2002), Detection of aerosol types over the East China Sea near Japan from four-channel satellite data, *Geophys. Res. Lett.*, *29*(17), 1836, doi:10.1029/2002GL015357.

Hoppel, W. A., G. M. Frick, and J. W. Fitzgerald (1996), Deducing droplet concentration and supersaturation in marine boundary layer clouds from surface aerosol measurements, *J. Geophys. Res.*, *101*(D21), 26,553–26,565.

Howell, S. G., A. D. Clarke, Y. Shinozuka, V. N. Kapustin, C. S. McNaughton, B. J. Huebert, S. Doherty, and T. Anderson (2006), Influence of relative humidity upon pollution and dust during ACE-Asia: Size distributions and implications for optical properties, *J. Geophys. Res.*, doi:10.1029/2004JD005759, in press.

Hudson, J. G., and S. S. Yum (2002), Cloud condensation nuclei spectra and polluted and clean clouds over the Indian Ocean, *J. Geophys. Res.*, *107*(D19), 8022, doi:10.1029/2001JD000829.

Huebert, B. J., T. Bates, P. B. Russell, G. Shi, Y. J. Kim, K. Kawamura, G. Carmichael, and T. Nakajima (2003), An overview of ACE-Asia: Strategies for quantifying the relationships between Asian aerosols and their climatic impacts, *J. Geophys. Res.*, *108*(D23), 8633, doi:10.1029/2003JD003550.

Jacob, D. J., J. H. Crawford, M. M. Kleb, V. S. Connors, R. J. Bendura, J. L. Raper, G. W. Sachse, J. C. Gille, L. Emmons, and C. L. Heald (2003), Transport and Chemical Evolution over the Pacific (TRACE-P) aircraft mission: Design, execution, and first results, *J. Geophys. Res.*, *108*(D20), 9000, doi:10.1029/2002JD003276.

Kaufman, Y. J., D. Tanre, and O. Boucher (2002), A satellite view of aerosols in the climate system, *Nature*, *419*(6903), 215–223.

Kim, D., B. Sohn, T. Nakajima, T. Takamura, T. Takemura, B. Choi, and S. Yoon (2004), Aerosol optical properties over east Asia determined from ground-based sky radiation measurements, *J. Geophys. Res.*, *109*, D02209, doi:10.1029/2003JD003387.

Lohmann, U., and G. Lesins (2002), Stronger constraints on the anthropogenic indirect aerosol effect, *Science*, *298*(5595), 1012–1015.

Lohmann, U., and G. Lesins (2003), Comparing continental and oceanic cloud susceptibilities to aerosols, *Geophys. Res. Lett.*, *30*(15), 1791, doi:10.1029/2003GL017828.

Ma, Y., et al. (2003), Characteristics and influence of biosmoke on the fine-particle ionic composition measured in Asian outflow during the Transport and Chemical Evolution Over the Pacific (TRACE-P) experiment, *J. Geophys. Res.*, *108*(D21), 8816, doi:10.1029/2002JD003128.

Ma, Y., et al. (2004), Intercomparisons of airborne measurements of aerosol ionic chemical composition during TRACE-P and ACE-Asia, *J. Geophys. Res.*, *109*, D15S06, doi:10.1029/2003JD003673.

Markowicz, K. M., P. J. Flatau, P. K. Quinn, C. M. Carrico, M. K. Flatau, A. M. Vogelmann, D. Bates, M. Liu, and M. J. Rood (2003), Influence of relative humidity on aerosol radiative forcing: An ACE-Asia experiment perspective, *J. Geophys. Res.*, *108*(D23), 8662, doi:10.1029/2002JD003066.

McNaughton, C. S., et al. (2004), Spatial distribution and size evolution of particles in Asian outflow: Significance of primary and secondary aerosols during ACE-Asia and TRACE-P, *J. Geophys. Res.*, *109*, D19S06, doi:10.1029/2003JD003528.

Mishchenko, M. I., B. Cairns, J. E. Hansen, L. D. Travis, R. Burg, Y. J. Kaufman, M. J. Vanderlei, and E. P. Shettle (2004), Monitoring of aerosol forcing of climate from space: Analysis of measurement requirements, *J. Quant. Spectrosc. Radiat. Transfer*, *88*(1–3), 149–161.

Moore, K. G., II, et al. (2004), A comparison of similar aerosol measurements made on the NASA P3-B, DC-8, and NSF C-130 aircraft during TRACE-P and ACE-Asia, *J. Geophys. Res.*, *109*, D15S15, doi:10.1029/2003JD003543.

Mukai, S., I. Sano, and M. Yasumoto (2003), Interrelation of aerosols, water vapor and clouds on a global scale, *Adv. Space Res.*, *32*(11), 2181–2190.

Nakajima, T., A. Higurashi, K. Kawamoto, and J. E. Penner (2001), A possible correlation between satellite-derived cloud and aerosol microphysical parameters, *Geophys. Res. Lett.*, *28*(7), 1171–1174.

Nakajima, T., et al. (2003), Significance of direct and indirect radiative forcings of aerosols in the East China Sea region, *J. Geophys. Res.*, *108*(D23), 8658, doi:10.1029/2002JD003261.

Ogunjobi, K. O., Z. He, K. W. Kim, and Y. J. Kim (2004), Aerosol optical depth during episodes of Asian dust storms and biomass burning at Kwangju, South Korea, *Atmos. Environ.*, *38*(9), 1313–1323.

Peixoto, J. P., and A. H. Oort (1996), The climatology of relative humidity in the atmosphere, *J. Clim.*, *9*(12), 3443–3463.

Quaas, J., O. Boucher, and F.-M. Bréon (2004), Aerosol indirect effects in POLDER satellite data and the Laboratoire de Météorologie Dynamique–Zoom (LMDZ) general circulation model, *J. Geophys. Res.*, *109*, D08205, doi:10.1029/2003JD004317.

Ramanathan, V., P. J. Crutzen, J. T. Kiehl, and D. Rosenfeld (2001), Atmosphere: Aerosols, climate, and the hydrological cycle, *Science*, *294*(5549), 2119–2124.

Redemann, J., S. J. Masonis, B. Schmid, T. L. Anderson, P. B. Russell, J. M. Livingston, O. Dubovik, and A. D. Clarke (2003), Clear-column closure studies of aerosols and water vapor aboard the NCAR C-130 during ACE-Asia, 2001, *J. Geophys. Res.*, *108*(D23), 8655, doi:10.1029/2003JD003442.

Remer, L. A., et al. (2002), Validation of MODIS aerosol retrieval over ocean, *Geophys. Res. Lett.*, *29*(12), 8008, doi:10.1029/2001GL013204.

Rissler, J., E. Swietlicki, J. Zhou, G. Roberts, M. O. Andreae, L. V. Gatti, and P. Artaxo (2004), Physical properties of the sub-micrometer aerosol over the Amazon rainforest during the wet-to-dry season transition comparison of modeled and measured CCN concentrations, *Atmos. Chem. Phys. Discuss.*, *4*, 3159–3225.

Rosenfeld, D. (2000), Suppression of rain and snow by urban and industrial air pollution, *Science*, *287*(5459), 1793–1796.

Rosenfeld, D., and G. Feingold (2003), Explanation of the discrepancies among satellite observations of the aerosol indirect effects, *Geophys. Res. Lett.*, *30*(14), 1776, doi:10.1029/2003GL017684.

Rosenfeld, D., Y. Rudich, and R. Lahav (2001), Desert dust suppressing precipitation: A possible desertification feedback loop, *Proc. Natl. Acad. Sci. U. S. A.*, *98*(11), 5975–5980.

Rosenfeld, D., R. Lahav, A. Khain, and M. Pinsky (2002), The role of sea spray in cleansing air pollution over ocean via cloud processes, *Science*, *297*(5587), 1667–1670.

Ru, J., N. Takeuchi, T. Uezono, S. Kaneta, M. Minomura, H. Kuze, T. Takamura, A. Higurashi, and T. Nakajima (2000), Optical properties of biomass burning smoke in South-east Asia studied by NOAA/AVHRR and ground-base monitoring, *Adv. Space Res.*, *25*(5), 1029–1032.

Rudich, Y., A. Sagi, and D. Rosenfeld (2003), Influence of the Kuwait oil fires plume (1991) on the microphysical development of clouds, *J. Geophys. Res.*, *108*(D15), 4478, doi:10.1029/2003JD003472.

Schwartz, S. E., and C. M. Benkovitz (2002), Influence of anthropogenic aerosol on cloud optical depth and albedo shown by satellite measurements and chemical transport modeling, *Proc. Natl. Acad. Sci. U. S. A.*, *99*(4), 1784–1789.

Sekiguchi, M., T. Nakajima, K. Suzuki, K. Kawamoto, A. Higurashi, D. Rosenfeld, I. Sano, and S. Mukai (2003), A study of the direct and indirect effects of aerosols using global satellite data sets of aerosol and cloud parameters, *J. Geophys. Res.*, *108*(D22), 4699, doi:10.1029/2002JD003359.

Svenningsson, B., et al. (2005), Hygroscopic growth and critical supersaturations for mixed aerosol particles of inorganic and organic compounds of atmospheric relevance, *Atmos. Chem. Phys. Discuss.*, *5*, 2833–2877.

Tang, I. N., A. C. Tridico, and K. H. Fung (1997), Thermodynamic and optical properties of sea salt aerosols, *J. Geophys. Res.*, *102*(D19), 23,269–23,276.

Tang, Y., et al. (2003), Influences of biomass burning during the Transport and Chemical Evolution Over the Pacific (TRACE-P) experiment identified by the regional chemical transport model, *J. Geophys. Res.*, *108*(D21), 8824, doi:10.1029/2002JD003110.

Tanre, D., L. A. Remer, Y. J. Kaufman, S. Mattoo, P. V. Hobbs, J. M. Livingston, P. B. Russell, and A. Smirnov (1999), Retrieval of aerosol optical thickness and size distribution over ocean from the MODIS airborne simulator during TARFOX, *J. Geophys. Res.*, *104*(D2), 2261–2278.

Twomey, S. (1991), Aerosols, clouds and radiation, *Atmos. Environ., Part A*, *25*(11), 2435–2442.

Vong, R. J., and D. S. Covert (1998), Simultaneous observations of aerosol and cloud droplet size spectra in marine stratocumulus, *J. Atmos. Sci.*, *55*(12), 2180–2192.

Wang, J., S. A. Christopher, F. Brechtel, J. Kim, B. Schmid, J. Redemann, P. B. Russell, P. Quinn, and B. N. Holben (2003), Geostationary satellite retrievals of aerosol optical thickness during ACE-Asia, *J. Geophys. Res.*, *108*(D23), 8657, doi:10.1029/2003JD003580.

Yum, S. S., and J. G. Hudson (2005), Adiabatic predictions and observations of cloud droplet spectral broadness, *Atmos. Res.*, *73*(3–4), 203–223.

Zhang, M., et al. (2003), Large-scale structure of trace gas and aerosol distributions over the western Pacific Ocean during the Transport and Chemical Evolution Over the Pacific (TRACE-P) experiment, *J. Geophys. Res.*, *108*(D21), 8820, doi:10.1029/2002JD002946.

Zhou, J., E. Swietlicki, H. C. Hansson, and P. Artaxo (2002), Submicrometer aerosol particle size distribution and hygroscopic growth measured in the Amazon rain forest during the wet season, *J. Geophys. Res.*, *107*(D20), 8055, doi:10.1029/2000JD000203.

V. Brekhovskikh, A. D. Clarke, S. Howell, V. N. Kapustin, and Y. Shinozuka, Department of Oceanography, School of Ocean and Earth Science and Technology, University of Hawaii at Manoa, 1000 Pope Rd., Honolulu, HI 96822, USA. (verab@soest.hawaii.edu; tclarke@soest.hawaii.edu; showell@soest.hawaii.edu; kapustin@soest.hawaii.edu; yohei@hawaii.edu)

A. Higurashi, Atmospheric Environment Division, National Institute for Environmental Studies, 16-2 Onogawa, Tsukuba, Ibaraki 305-8506, Japan. (hakiko@nies.go.jp)

T. Nakajima, Center for Climate System Research, University of Tokyo, 4-6-1 Komaba, Meguro-ku, Tokyo 153-8904, Japan. (teruyuki@ccsr.u-tokyo.ac.jp)